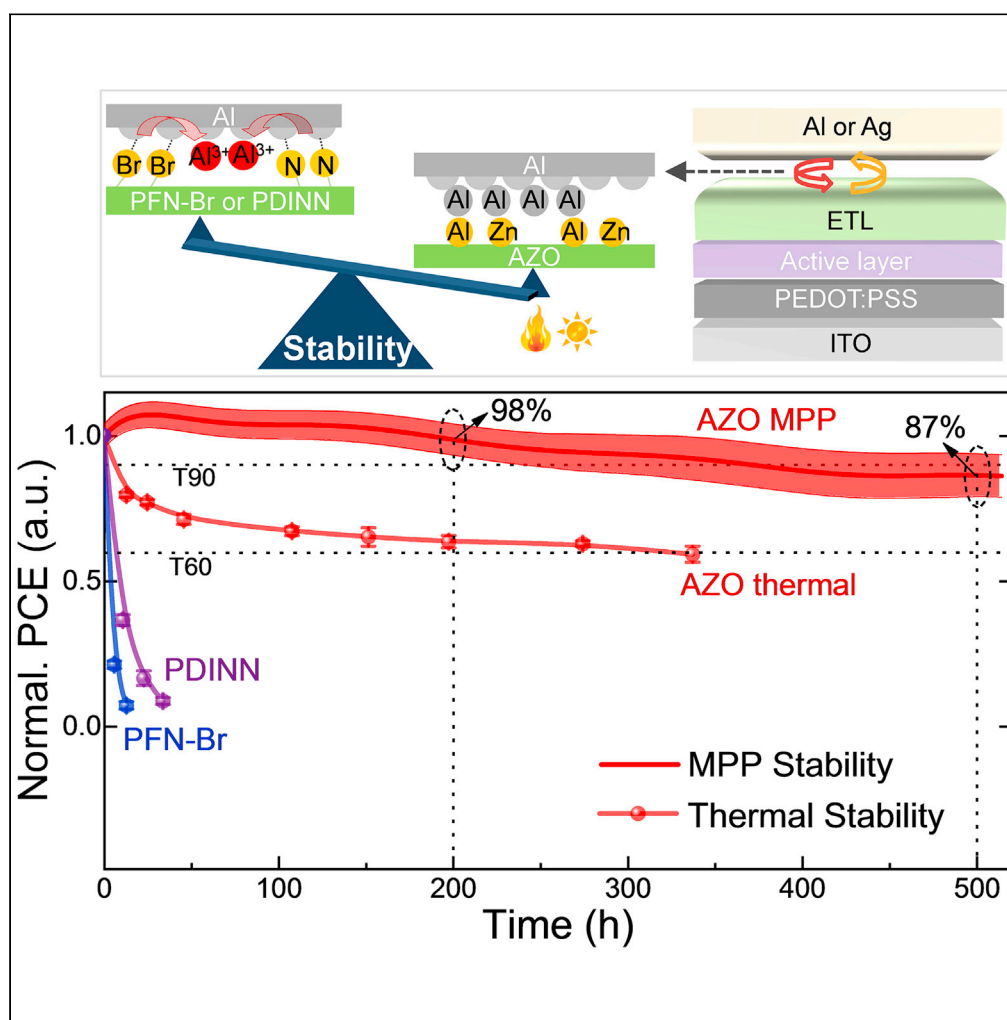


Article

Efficient organic solar cells with superior stability based on PM6:BTP-eC9 blend and AZO/Al cathode



Zhipeng Yin, Sikai Mei, Pengcheng Gu, Hai-Qiao Wang, Weijie Song

hqwang@nimte.ac.cn (H.-Q.W.)
weijiesong@nimte.ac.cn (W.S.)

Highlights

Electron transport layers and electrode metals are screened to study cell stability

Strong correlation between cathode and device stability is demonstrated

AZO/Al-based organic solar cells deliver high efficiency and superior stability

Article

Efficient organic solar cells with superior stability based on PM6:BTP-eC9 blend and AZO/Al cathode

Zhipeng Yin,¹ Sikai Mei,¹ Pengcheng Gu,¹ Hai-Qiao Wang,^{1,2,3,*} and Weijie Song^{1,*}

SUMMARY

Although efficiency over 18% has been achieved, the real application of organic solar cells is still impeded by inferior stability because of degradation and limited studies. Here we report efficient normal structure organic solar cells delivering promising stability under different conditions, based on PM6:BTP-eC9 blend and AZO/Al cathode. The impact of cathode on device stability is systematically studied by screening the leading electron transporting layers i.e., AZO, PFN-Br, PDINN, and metal electrodes (Al and Ag). Strong correlation between cathode and stability is demonstrated. The optimal AZO/Al-cathode device delivers the best efficiency of 15.76%, with shelf-stability of T83 > 1,200 h, thermal stability of T60 > 300 h, and MPP operational stability of T87 > 500 h. As far as we know, this is the best stability achieved for PM6:Y6/derivative cells in literature so far, based on well-studied simple cathode system and without any tailoring/dopant for the active blend.

INTRODUCTION

Organic solar cells (OSCs) can be solution-processed on flexible substrates at low temperatures, enabling fast and inexpensive manufacturing. Thus they have attracted great attention in past decades. Huge progress in power conversion efficiency (PCE) has been achieved since advances in material and device engineering (Zheng et al., 2019). Especially, the shifting from traditional utilization of fullerene/derivatives as electron acceptors to non-fullerene acceptors (NFAs) (Hou et al., 2018; Lin et al., 2015), for instance, NFA Y6 (Yuan et al., 2019) and derivatives (Cheng et al., 2018), boosts the state-of-the-art efficiency to over 18% (Liu et al., 2020b; Zhan et al., 2021). Despite the great achievements in device efficiency, the commercialization of OSCs is still limited by their relatively low stability, owing to degradations and limited study (Mateker and McGehee, 2017; Rafique et al., 2018). Understanding and overcoming the degradation mechanism/problems are essential. Developing efficient OSCs with promising thermal and long-term operational stability is greatly demanded by the community.

Degradation can occur at each part of a device stack, for instance, active blend, interlayer, and electrode because of extrinsic (e.g., environmentally induced water and oxygen) or intrinsic (e.g., light, heat, and electric bias) factors (Mateker and McGehee, 2017). By which, morphology change, chemical reaction, and energy level mismatch could happen at all function layers or/and their contact, thus degrading the device performance. And in the real application, the performance decay is usually a result of a complex interplay of these multiple processes (Labanti et al., 2021).

Most stability studies have been focused on fullerene-based cells (Cheng et al., 2016; Jørgensen et al., 2012; Li et al., 2017; Zhang et al., 2019). But relatively less has been dedicated to efficient NFA-based systems about this topic (Du et al., 2020). To promote the stability of NFA-based OSCs, different strategies including tailoring of NFA (Du et al., 2020; Hu et al., 2020; Labanti et al., 2021) and donor (Zhang et al., 2021), designing new active materials (Bin et al., 2020), ternary-blend method (Yang et al., 2020), utilization of stabilizer/dopant (Linglong Ye et al., 2020; Zhang et al., 2019), and interface engineering (Lin et al., 2020; Yao et al., 2020), have been adopted. Focusing on photo-stability, Brabec (Du et al., 2020) and coworkers systematically studied the PM6/derivatives: IT-4F blend systems. It is concluded that NFA aggregation because of incompatibility with donor material contributes to performance loss. T80 (80% of the initial PCE) lifetime of ~1,300 h can be obtained for optimal inverted devices (ITO/ZnO/blend/MoO₃/Al) under

¹Ningbo Institute of Materials Technology and Engineering, Chinese Academy of Sciences, Ningbo 315201, China

²NingboTech University, Ningbo, 315100, China

³Lead contact

*Correspondence: hqwang@nimte.ac.cn (H.-Q.W.), weijiesong@nimte.ac.cn (W.S.)

<https://doi.org/10.1016/j.isci.2021.103027>



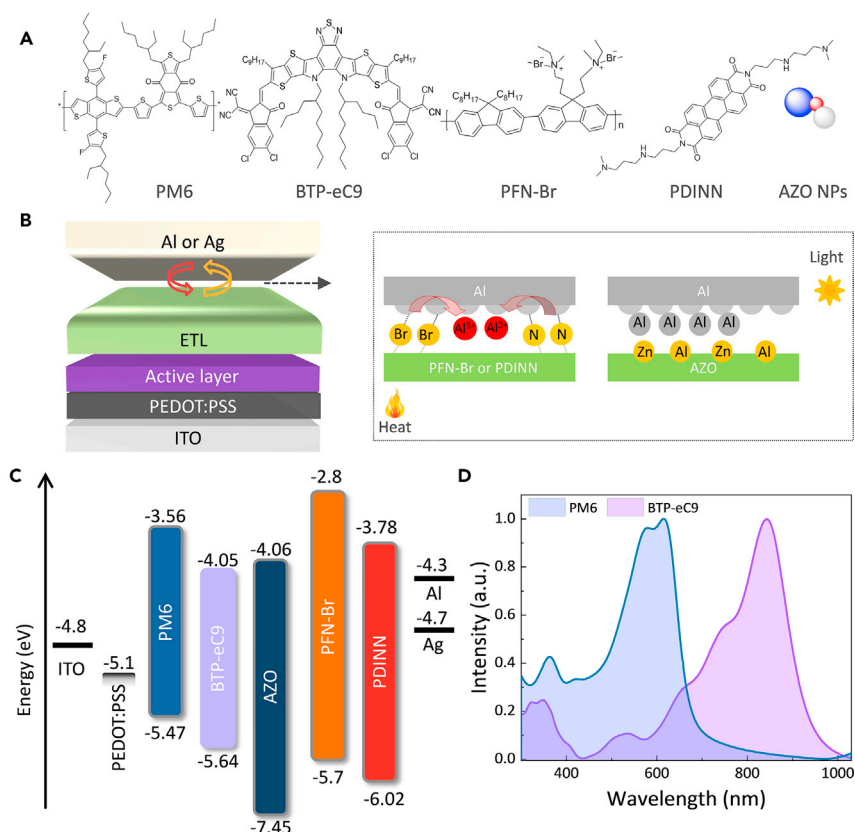


Figure 1. Material property and schematic depiction of cathode contact

(A) Chemical structure of polymer donor PM6, NFA BTP-eC9, and interfacial materials utilized.

(B) Configuration of normal device structure (ITO/PEDOT:PSS/PM6:BTP-eC9/ETL/Metal) adopted in the study and schematic diagram of contact at ETL/Metal.

(C) Energy level alignment of the materials used in devices.

(D) Absorption spectra of the polymer donor PM6 and NFA BTP-eC9.

illumination and open circuit condition. With a similar inverted structure, Kim et al. (Labanti et al., 2021), optimized the interaction between ITIC and donor PBDB-T by selenium-substitution on ITIC to stabilized the blend, thus promoting the device photo-stability.

Thermal stress is considered another sensitive and key factor causing performance decay as its strong impact on blend nanoscale morphology by phase separation (Speller et al., 2019; Zhang et al., 2017). To improve device thermal-stability, polymer donors with different molecular weights were utilized for blend (PBDB-T4Cl5S:Y6) morphology optimization by Huang et al. (Zhang et al., 2021). Much improved shelf- and thermal-stability were accomplished with a medium molecular weight owing to optimal miscibility between donor and Y6. Based on the ternary strategy, by adding a third polymer acceptor PZI into the PM6:BTBT-2Cl blend to improve crystallinity, Min and coworkers (Yang et al., 2020) greatly enhanced the thermal stability of the device in a normal structure.

Based on those studies focused on curing the blend morphology change, although long-term stability of 10-year-lifetime is promised (Du et al., 2019), NFA-based OSCs still suffer from significant degradations (Du et al., 2020; Mateker and McGehee, 2017). Besides active blend, we consider interlayer, for instance, the electron transporting layer (ETL) and electrode present significant influence on performance stability as well (Lin et al., 2020; Yao et al., 2020) because they play a key role in determining device polarity and charge extraction efficiency (Yin et al., 2016). Yao et al. (Yao et al., 2020), demonstrated that cathode significantly influences not only efficiency but also storage stability. However, their impact on device stability has received limited attention so far. Developing/screening efficient cathode systems providing high stability for OSC, and understanding the mechanisms are in great demand.

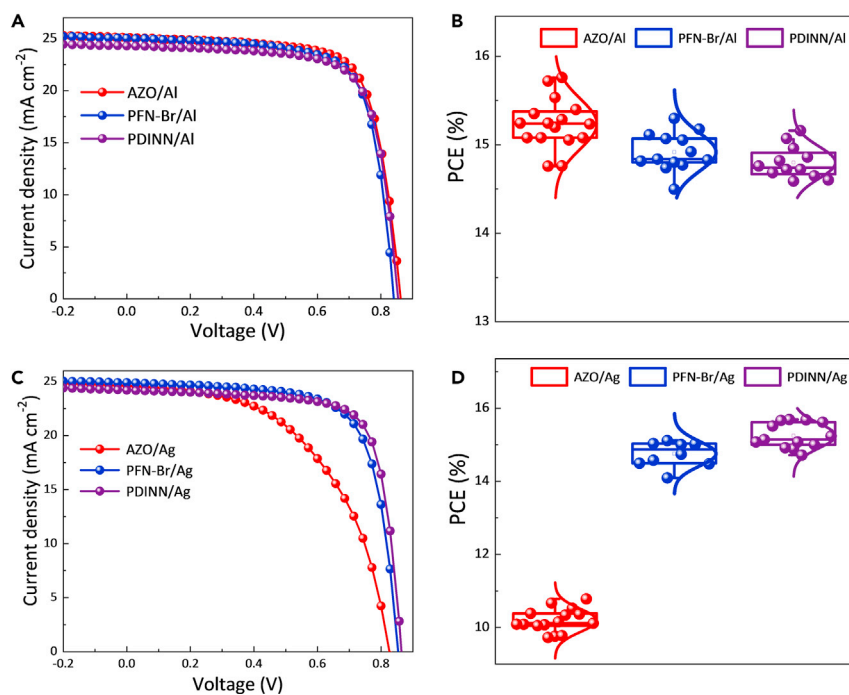


Figure 2. Device performance based on different cathodes

(A and B) J-V curves and efficiency statistics of devices based on AZO/Al, PFN-Br/Al, or PDINN/Al cathode.

(C and D) J-V curves and efficiency statistics of devices based on AZO/Ag, PFN-Br/Ag, or PDINN/Ag cathode. The statistics are based on 14 individual cells.

In this work, we report efficient PM6:BTP-eC9 (Cui et al., 2020) organic solar cells delivering promising stability under different conditions. The devices are fabricated in the normal structure of ITO/PEDOT:PSS/PM6:BTP-eC9/ETL/Metal (Liu et al., 2017). Based on representative electron transporting materials (ETMs) AZO (Liu et al., 2017), PFN-Br (Cui et al., 2020), and PDINN (Yao et al., 2020) as ETL and the most typical metal electrode Al and Ag, the impact of the cathode (ETL/Metal) on device stability are systematically studied. Stability details are revealed and the underlying mechanisms are proposed and discussed. The optimal AZO/Al-cathode device delivers the best efficiency of 15.76%, with shelf-stability of T83 > 1,200 h, thermal-stability of T60 > 300 h, and MPP operational stability of T87 > 500 h. As far as we know, this is one of the best stabilities achieved for efficient polymer:NFA OSCs in literature so far (Classen et al., 2019; Yang et al., 2020), based on well-studied simple cathode system and without any tailoring/dopant for active blend.

RESULTS AND DISCUSSION

The chemical structure of polymer donor PM6 (Zhang et al., 2015), NFA BTP-eC9 (Cui et al., 2020), and interfacial materials, and the adopted normal device structure (ITO/HTL/PM6:BTP-eC9/ETL/Metal) are presented in Figure 1. Poly(3,4-ethylene dioxythiophene) polystyrene sulfonate (PEDOT:PSS) is utilized as the hole transporting layer (HTL). Three representative ETLs i.e., AZO, PFN-Br, and PDINN, combined with metal electrode Al or Ag, are adopted to compose the cathode and for comparison. Figure 1B depicts the schematic diagram of contact between ETL and electrode, showing possible interactions that correlated to the device degradation. Energy level alignment of all the materials used in devices and the absorption spectra of active materials are presented in Figures 1C and 1D.

Performance parameters of the device with different cathode are summarized in Figure 2 and Table 1. Combined with metal Al electrode, all three leading ETLs deliver a decent PCE of over 15%. A champion PCE of 15.76% is obtained based on AZO/Al cathode, with an open circuit voltage (V_{OC}) of 0.86 V, short circuit current density (J_{SC}) of 25.10 mA cm⁻², and fill factor (FF) of 72.8%. When combined with Ag electrode, the ETLs provide comparable efficiency of over 15% again except for AZO. The AZO/Ag cathode

Table 1. Parameters of different cathode-based OSCs

EHL	Metal	V_{OC} (V)	J_{SC} (mAcm^{-2})	FF (%)	PCE (%)	R_S (Ωcm^2)	R_{sh} ($\text{k}\Omega\text{cm}^2$)
AZO	Al	0.86	25.10	72.8	15.76 (15.22)	56.9	15.54
PFN-Br		0.84	25.01	72.7	15.29 (14.69)	68.9	26.08
PDINN		0.85	24.29	73.0	15.15 (14.61)	82.0	30.09
AZO	Ag	0.83	24.55	53.1	10.78 (10.19)	103.5	8.73
PFN-Br		0.85	24.87	71.2	15.11 (14.75)	82.3	26.96
PDINN		0.86	24.21	75.0	15.69 (15.01)	61.4	24.67

The average PCE in parentheses was based on 14 individual devices.

delivers PCE of only 10.78% due to slightly suppressed V_{OC} and dramatically lowered FF by imperfect contact of AZO/Ag (Mihailetchi et al., 2003). This is evidenced by the high series resistance and low shunt resistance (Table 1), further confirmed by the sheet resistance (Table S1).

First, the shelf/storage stability of different-cathode-based devices was tested in N_2 -filled glove box at room temperature (Figure 3, left column). Almost all devices based on the leading ETLs and metal electrodes presented a fairly stable performance in a long-term shelf-storage under indoor daylight (ID-DL) in the glove box. The best shelf-stability of the device is achieved with PDINN/Ag cathode, retaining 95% of its initial efficiency (T95) in 50 days i.e. 1,200 h (T95 > 1,200 h). The PDINN/Al, AZO/Al, and PFN-Br/Ag cathode devices maintained over 80% of their initial efficiency in the same time scale (T80 > 1,200 h). Slightly faster performance decay was observed for AZO/Ag cathode device, with 75% of initial efficiency maintained in 1,200 h. And the PFN-Br/Al device presented a relatively fast decay with 37% of the initial value remained in 1,200 h, which is consistent with the result in other reports (Cui et al., 2020; Sun et al., 2021). To understand the efficiency decay in shelf-storage, the performance parameters including V_{OC} , J_{SC} , and FF of devices were presented in Figure S1. It is concluded that for Al-electrode-based devices, the decay can be influenced by all the parameters (Figures S1A–S1C). Especially, the decay of the PFN-Br/Al-cathode device is directly ascribed to its quick FF loss (Figure S1C). While differently in Ag-electrode-based devices, the J_{SC} s remain quite stable, which could be related to the stable reflectivity of Ag electrodes when compared to Al electrodes (Figure S7). V_{OC} loss (Figure S1D) is the main reason causing the efficiency decay of AZO/Ag devices. And again the FF loss (Figure S1F) should mainly account for the PFN-Br/Ag device decay.

The thermal-stability test was conducted for the different cathode devices under 85°C thermal stress in N_2 atmosphere. As shown in Figure 3 (right column), a much-accelerated decay process was recorded for all devices, compared to their shelf-stability. Combined with the Al electrode, both PFN-Br and PDINN ETL-based devices degraded fast to failure within a few tens of hours (Figure 3B). This is consistent with the results reported in literatures (Cui et al., 2020; Sun et al., 2021; Yao et al., 2020). Relatively more stable performance was recorded for AZO/Al-cathode device. It maintained 60% of initial efficiency for over 300 hours (T60 > 300 h) under thermal stress. When combined with the Ag electrode, the devices presented overall improved thermal stability compared to the Al-electrode-based cells (Figure 3D). And again the AZO-based device delivered the best thermal stability. These results indicate that AZO ETL shows superiority in achieving good thermal stability for this type of OSCs, compared to PFN-Br and PDINN ETLs. This could be ascribed to the better morphological and chemical stability (Hewlett and McLachlan, 2016; Liu et al., 2016) of AZO as inorganic material than the organic molecules, under thermal conditions. Different from shelf-storage, all parameters including V_{OC} , J_{SC} , and FF showed a specific decrease under thermal stress (Figure S2). The synergetic effect of these decreases resulted in the accelerated decay of devices under thermal stress. We consider that the different decay processes by cathode variation could be related to morphology and/or chemical changes at the cathode, which will be discussed later. It should be noted that under thermal stress, almost zero J_{SC} loss was recorded again, for AZO/Al and AZO/Ag cathode devices (Figures S2B and S2E).

Operational stability is one of the most essential parameters for the practical application of OSCs. Figure 4 shows the long-term operational stability of devices under maximum power point (MPP) tracking and 1 sun illumination in N_2 atmosphere. Interestingly, superior MPP operational stability is obtained for AZO-Al and PDINN/Al cathode devices, with T98 > 200 h and T90 > 200 h respectively. The PFN-Br/Al device presents

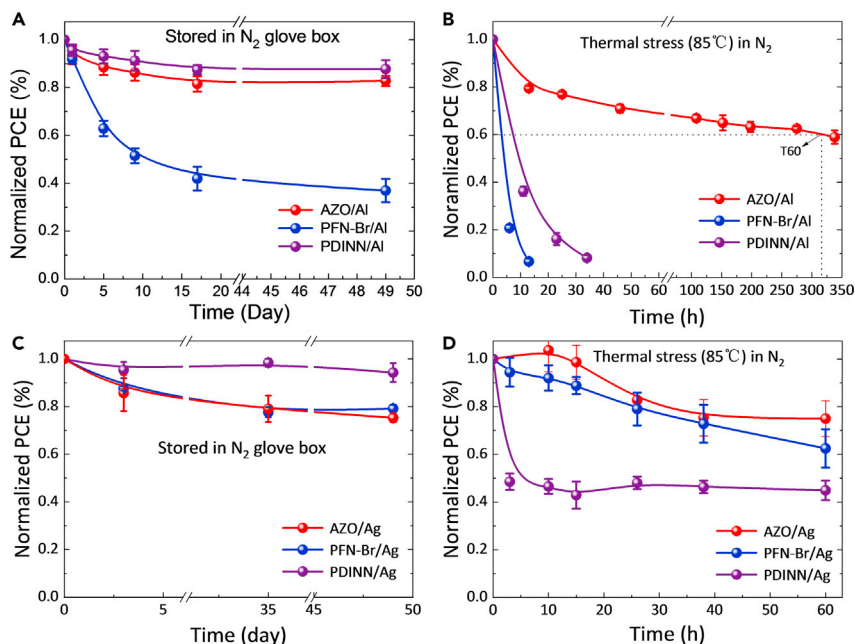


Figure 3. Efficiency decay of devices with different cathodes

(A and C) Efficiency decay of different-cathode-based devices under shelf-storage.

(B and D) Efficiency decay of different-cathode-based cells under $85^\circ C$ thermal stress. (Aging test is conducted in N_2 atmosphere in the glove box. The standard deviation is based on 8 individual devices.)

relatively fast performance decay ($T_{40} \approx 130$ h) under MPP aging. When combined with Ag electrode, the devices provide comparable but slightly lowered operational stability (Figure 4B), with 70–90% of initial efficiency maintained in 200 hours. Similar to shelf-storage, the efficiency decay of the PFN-Br device is mainly

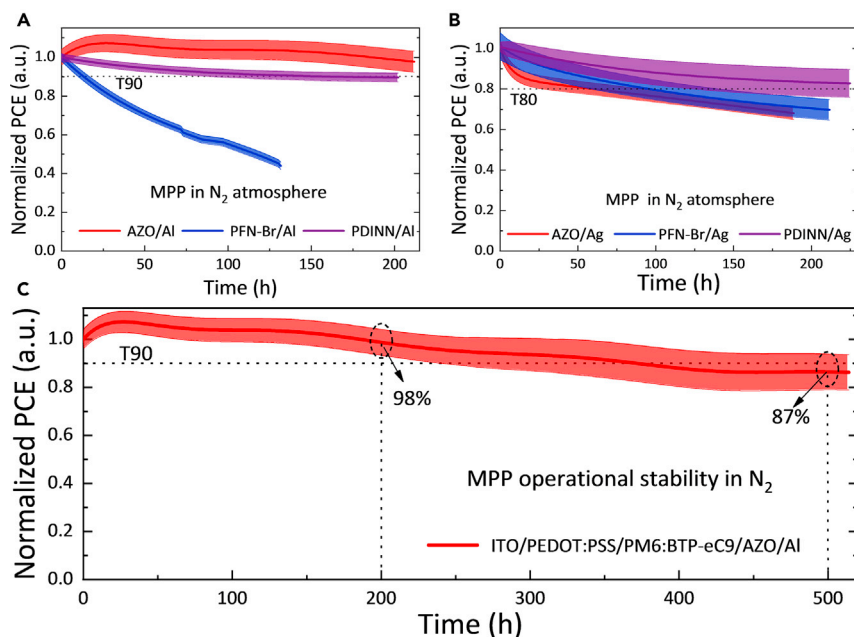


Figure 4. Operational stability of cells with different cathodes

(A–C) Operational stability of different cells under maximum power point (MPP) tracking in N_2 atmosphere, with the cathode of (A) ETL/Al, (B) ETL/Ag, and (C) AZO/Al. (The deviation is based on 4 individual devices.)

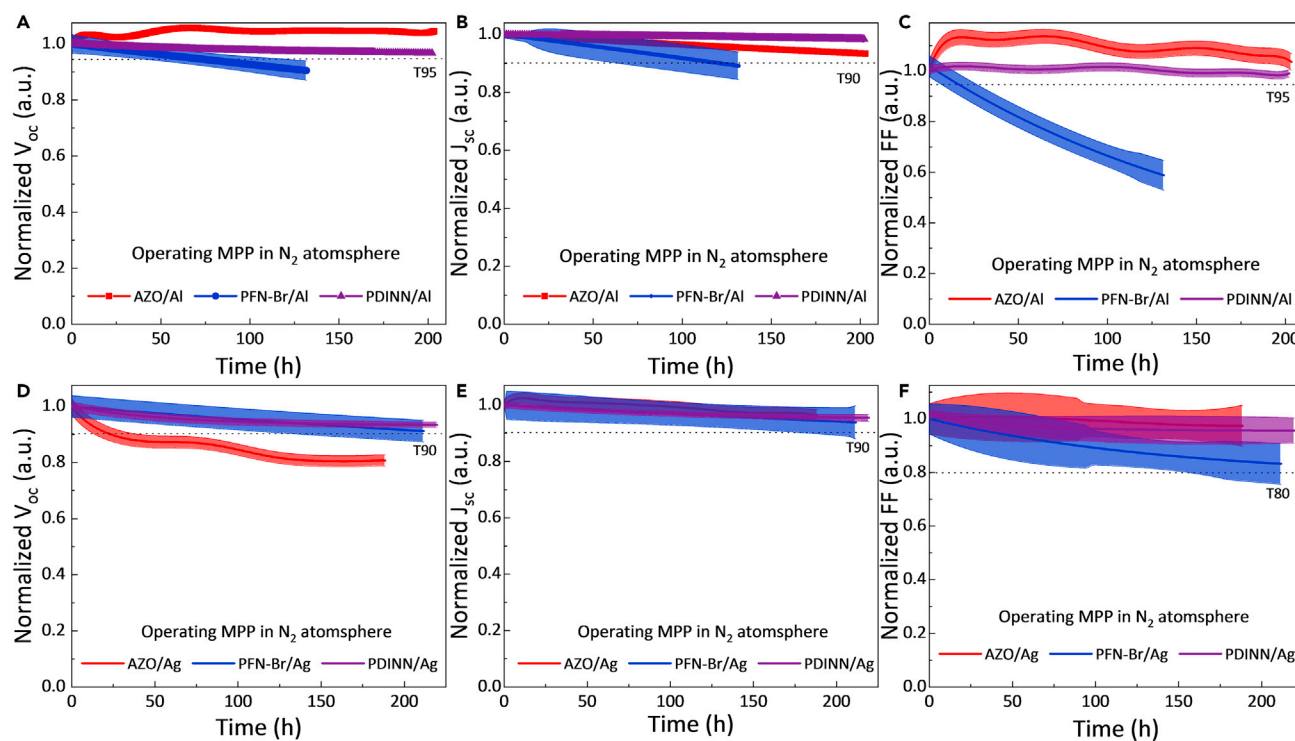


Figure 5. Decay of performance parameters

(A–F) Parameters decay of OSCs with different ETL (AZO, PFN-Br or PDINN) and metal electrode (Al or Ag), under MPP operation: (A and D) V_{OC} ; (B and E) J_{SC} ; (C and F) FF. (The deviation is based on 4 individual devices.)

dominated by FF loss (Figure 5C); the decay of the AZO/Ag device is more determined by the V_{OC} loss (Figure 5D). The best MPP operational stability is recorded based on the AZO/Al device (ITO/PEDOT:PSS/PM6:BTP-eC9/AZO/Al) (Figure 4C), with $T_{98} > 200$ h and $T_{87} > 500$ h confirmed. To the best of our knowledge, this is the best long-term operational stability of PM6:Y6/derivatives OSCs reported in the literature so far. As a comparison, typical stability parameters of NFA-based binary OSCs in literature are summarized in Table 2, together with the devices in this work. It should be noted that the whole aging process has been conducted in a moisture-free and oxygen-free atmosphere.

Because the same fabrication process has been utilized to prepare the active layer of all the devices, we consider the difference in efficiency decay of devices must be related to their cathode property, which is the sole part varied in the devices. Different properties of ETLs and/or electrode metals would cause different morphology and/or chemical changes at the cathode, and contribute to different degradation. To explore the details and understand the degradation, morphology, and chemical/electronic state at interface of ETL/electrode were characterized. Al and Ag films (100 nm) on glass substrate were treated in warmed (85°C) AZO, PFN-Br, and PDINN solutions (Figure 6A) to simulate and accelerate the interaction between ETL and metal electrode in the device. Obvious morphology change was observed for metal films. Especially, large morphology and color change were demonstrated for Al films treated with PFN-Br and PDINN solutions (Figure 6B), compared to the control film (Al-air), suggesting strong interaction between Al and the PFN-Br and PDINN molecules. While kept in AZO solution, the Al film presented a nonobvious morphology/color change. This could explain the different thermal stability of their corresponding devices (Figure 3B). A similar phenomenon but overall much slighter morphology change was observed for Ag films, compared to Al films. This is consistent with the improved thermal stability of their corresponding devices (Figures 3B and 3D). Again, a relatively larger morphology change was recorded for Ag film treated by organic solutions, but almost no change was recorded for the AZO-solution-treated one. This could be ascribed to the better chemical stability of Ag than Al, probably because of higher work-function. To exclude the influence of solvents, fresh metal Al and Ag films were treated by using pure methanol and trifluoroethanol (TFE) solvent, respectively, at 85°C. No obvious morphology change was observed

Table 2. Typical stability parameters of NFA-based binary OSCs in literature, together with our devices

Active layer (AL)	Device	Conditions	Aged time	Best PCE (%)	Remain (%)	References
PM6:Y6	ITO/PEDOT:PSS/AL/PDINN/Ag	Dark-Shelf	1,200 h	17.2	90	Nat. Comm. 2020 (Yao et al., 2020)
PM6:Y6	ITO/PEDOT:PSS/AL/DPO/Al	1 Sun	225 h	15.2	40	ACS Energy Lett. 2020 (Gasparini et al., 2020)
PM6:PTIC	ITO/ZnO/AL/MoO ₃ /Ag	1 Sun	50 h	10.27	70	Nat. Com. 2019 (Yu et al., 2019)
PM6:IT-4F	ITO/ZnO/AL/MoO ₃ /Al	1 Sun	1,300 h	10.8	78	Adv. Mat. 2020 (Du et al., 2020)
PM6:IT-4F	ITO/ZnO/AL/MoO ₃ /Ag	100°C	34 h	12.12	75	ACS Energy Let. 2020 (Park et al., 2020)
PM6:BTP-eC9	ITO/PEDOT:PSS/AL/PFN-Br/Al	50°C	100 h	17.8	58	Adv. Mat. 2020 (Cui et al., 2020)
PM6:BTMT-2Cl	ITO/PEDOT:PSS/AL/PDINO/Al	110°C	120 h	13.13	48	Nat. Comm. 2020 (Yang et al., 2020)
PM6:N3	ITO/PEDOT:PSS/AL/PFN-Br/Ag	MPP	50 h	15.94	20	ACE Energy Lett. 2020 (Lin et al., 2020)
	ITO/2PACz/AL/PFN-Br/Ag		120 h	16.6	74	
PBQ-QF:io-IDTBR	ITO/ZnO/Ba(OH) ₂ /AL/MoO ₃ /Al	@V _{OC} or @J _{SC}	1000 h	8.08	80	Adv. Energy. Mater. 2019 (Classen et al., 2019)
B1:BTP-eC9	ITO-Cl/AL/Al	Shelf	200 h	14.86	72	Energy Environ. Sci. 2021 (Sun et al., 2021)
		1 Sun	200 h		40	
PM6:BTP-eC9	ITO/PEDOT:PSS/AL/AZO/Al	Shelf	1,200 h	15.76	83	This work
		85°C	318 h		60	
		MPP	513 h		87	

compared to the ETL-solution-treated films (Figure S3). This demonstrates that the interactions between ETL molecule and electrode metal contribute to cathode degradation, thus device performance.

To further understand the cathode changes, X-ray photoelectron spectroscopy (XPS) was conducted at the interface (Figure 7). Figure 7A shows the Al 2p spectra of the treated films. Both metallic Al (72.2 eV) and Al₂O₃ (74.2 eV) are detected at the surface of the control film (Al-air) owing to exposure in air, which matches well the theoretic peak positions (Liu et al., 2020a). After being treated with PFN-Br and PDINN solution, the Al (2p) metallic core level (Al 2p_{3/2}) (Figure 7A) shifts toward higher binding energy (from 72.2 to 72.4 eV) and the Al 2p_{1/2} peak almost disappears, suggesting electron transfer from metal atoms to organic molecules by strong chemical reaction. When treated with AZO solution, this energy shift is not measured and both core line peaks (Al 2p_{1/2} and 3/2) retained, suggesting no chemical reactions. A similar phenomenon is observed for Ag films (Figure 7B). A clear shift of Ag 3d core line spectra toward higher binding energy is observed for all ETL-treated Ag electrodes, but with an overall more gentle process compared to the Al electrode (Figure 6B). The biggest shift is recorded for PFN-Br treated Ag films, probably because of more halide of this material (Wang et al., 2021; Zhao et al., 2016). These results indicate a stronger chemical interaction between the metal electrode and the organic ETL molecules than between metal and AZO (as depicted in Figure 1B) under thermal conditions, which is consistent with the recorded thermal stability of the devices. Further, as for the chemical interaction or reaction mechanism, we consider it is related to redox reactions between metal and haloid (Wang et al., 2021; Zhao et al., 2016), or amino group, as depicted in Figure 1B and evidenced by the morphology changes of metal films (Figures 6 and S4–S7).

Conclusions

In summary, we report efficient PM6:BTP-eC9 OSCs delivering promising long-term stability, with a normal structure of ITO/PEDOT:PSS/PM6:BTP-eC9/AZO/Al. Representative ETLs (AZO, PFN-Br, and PDINN) and the most typical metal electrodes (Al and Ag) are screened to compose the cathode (ETL/Metal) and for comparison. The impact of cathode on device performance and stability is systematically studied. Relative details are revealed and possible reason/mechanisms are discussed. Fairly stable performance (T₈₀ > 1,200 h) is expectable for the leading ETLs-based cells under shelf-storage. The decay is much accelerated for devices under thermal stress, especially for organic ETL/Al devices owing to chemical reactions at the cathode. The optimal AZO/Al device delivers the best efficiency of 15.76%, with promising shelf-stability of T₈₀ > 1,200 h, thermal-stability of T₆₀ > 300 h, and MPP operational stability of T₈₇ > 500 h. This is the best stability achieved for efficient PM6:Y6/derivative cells in literature so far, without any tailoring/dopant

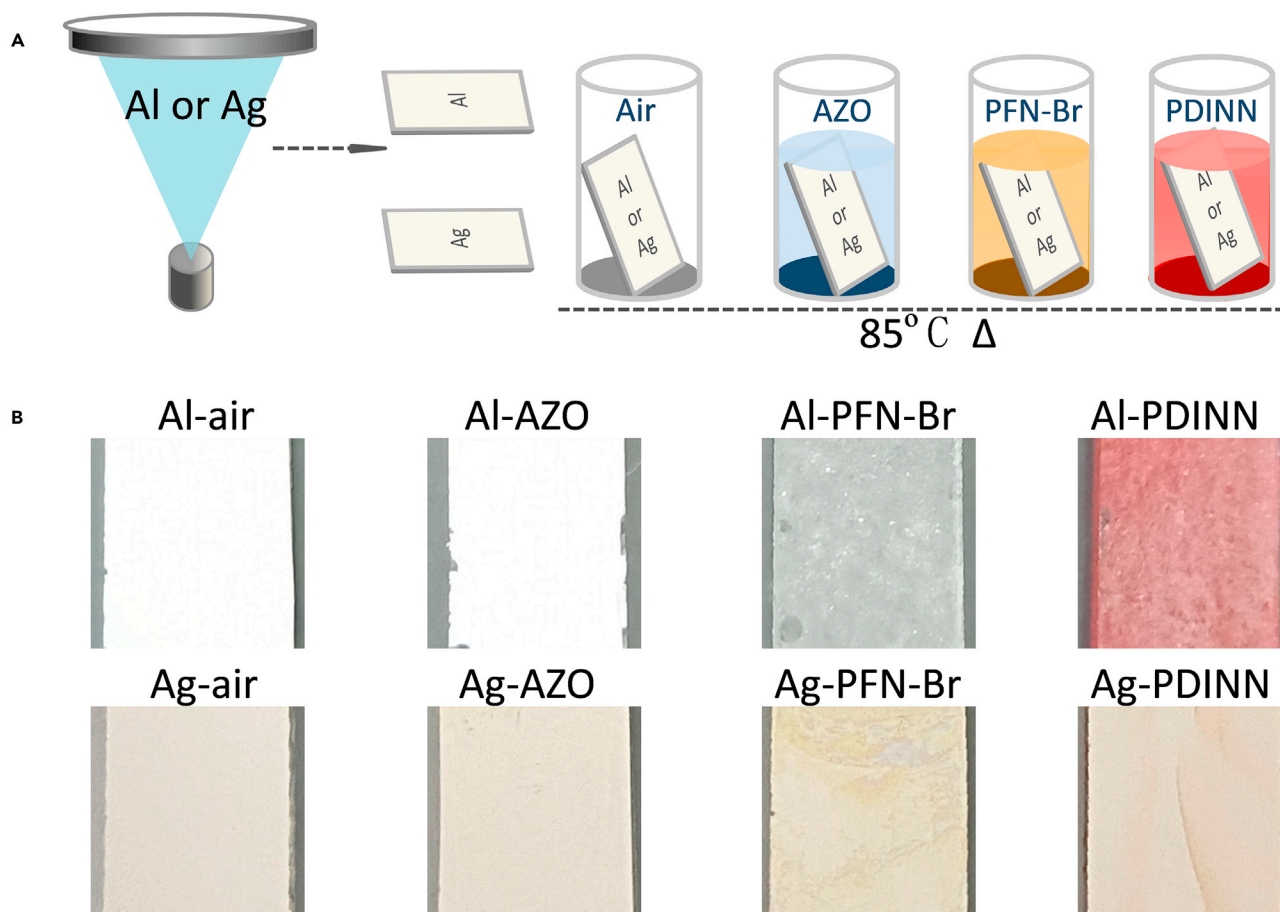


Figure 6. Morphological characteristics of cathodes

(A) Thermal-evaporated 100 nm Al or Ag film on the glass substrate, kept in AZO, PFN-Br, and PDINN solutions to simulate the reactions between metal and the ETL under 85°C. The one kept in the air is for control.

(B) Photo of the films after treatment by different ETL solutions.

for the active blend. This cathode system could fulfill the requirement of commercialization of OSC, because of its low cost and material abundance. This study provides insight into cathode impact on device degradation and strategy to promote the stability of OSCs.

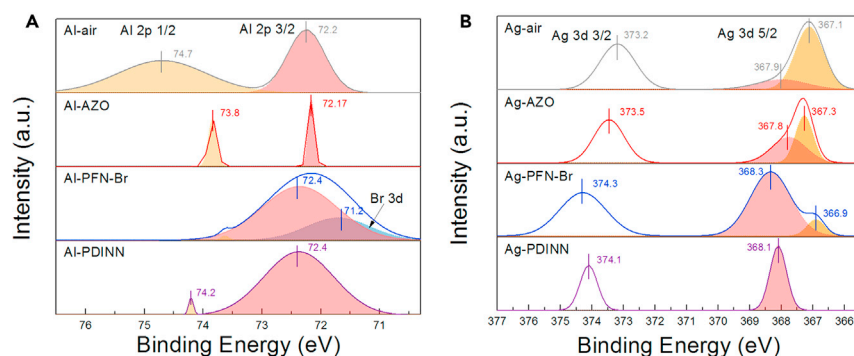


Figure 7. XPS characteristics of cathodes

(A and B) Core line XPS spectra of (A) Al 2p of the Al film and (B) Ag 3d of the Ag film, treated by AZO, PFN-Br, and PDINN solutions.

Limitations of the study

In the current study, organic solar cells that were used are based on leading electron transporting materials and typical electrode metals. Other representative electron selecting materials e.g., PDINO, DPO and PNDIT-F3N are not included. The fabricated organic solar cells based on PM6:BTP-eC9 blend provide relatively lower efficiency compared to those top values of the cells reported in literature.

STAR★METHODS

Detailed methods are provided in the online version of this paper and include the following:

- KEY RESOURCE TABLE
- RESOURCE AVAILABILITY
 - Lead contact
 - Materials availability
 - Data and code availability
- METHOD DETAILS
 - Materials and reagents
 - Device fabrication
 - Characterizations
- QUANTIFICATION AND STATISTICAL ANALYSIS

SUPPLEMENTAL INFORMATION

Supplemental information can be found online at <https://doi.org/10.1016/j.isci.2021.103027>.

ACKNOWLEDGMENTS

This work was supported by the funding of Ningbo S&T Innovation 2025 Major Special Program (No.2018B10055), Ningbo, China and Jiangsu Collaborative Innovation Center of Photovoltaic Science and Engineering, Changzhou, China.

AUTHOR CONTRIBUTIONS

Conceptualization, H.-Q. and W.J.; Methodology, Z.P., S.K. and H.-Q.; Investigation, Z.P., S.K., P.C. and H.-Q.; Writing-Original Draft, Z.P.; Writing & Editing, Z.P. and H.-Q.; Funding Acquisition, H.-Q. and W.J.; Supervision, H.-Q. and W.J.

DECLARATION OF INTERESTS

The authors declare no competing interests.

Received: May 13, 2021

Revised: July 7, 2021

Accepted: August 19, 2021

Published: September 24, 2021

REFERENCES

- Bin, H., Wang, J., Li, J., Wienk, M.M., and Janssen, R.A.J. (2020). Efficient electron transport layer free small-molecule organic solar cells with superior device stability. *Adv. Mater.* 33, 2008429.
- Cheng, P., Yan, C.Q., Lau, T.K., Mai, J.Q., Lu, X.H., and Zhan, X.W. (2016). Molecular lock: a versatile key to enhance efficiency and stability of organic solar cells. *Adv. Mater.* 28, 5822–5829.
- Cheng, P., Li, G., Zhan, X.W., and Yang, Y. (2018). Next-generation organic photovoltaics based on non-fullerene acceptors. *Nat. Photon.* 12, 131–142.
- Classen, A., Heumueller, T., Wabra, I., Gerner, J., He, Y., Einsiedler, L., Li, N., Matt, G.J., Osvet, A., Du, X., et al. (2019). Revealing hidden UV instabilities in organic solar cells by correlating device and material stability. *Adv. Energy Mater.* 9, 1902124.
- Cui, Y., Yao, H.F., Zhang, J.Q., Xian, K.H., Zhang, T., Hong, L., Wang, Y.M., Xu, Y., Ma, K.Q., An, C.B., et al. (2020). Single-Junction organic photovoltaic cells with approaching 18% efficiency. *Adv. Mater.* 32, 1908205.
- Du, X., Heumueller, T., Gruber, W., Classen, A., Unruh, T., Li, N., and Brabec, C.J. (2019). Efficient polymer solar cells based on non-fullerene acceptors with potential device lifetime approaching 10 years. *Joule* 3, 215–226.
- Du, X., Heumueller, T., Gruber, W., Almora, O., Classen, A., Qu, J., He, F., Unruh, T., Li, N., and Brabec, C.J. (2020). Unraveling the microstructure-related device stability for polymer solar cells based on nonfullerene small-molecular acceptors. *Adv. Mater.* 32, 1908305.
- Gasparini, N., Paleti, S.H.K., Brandt, J., Cai, G., Zhang, G., Wadsworth, A., Lu, X., Yip, H.-L., McCulloch, I., and Baran, D. (2020). Exploiting ternary blends for improved photostability in high-efficiency organic solar cells. *ACS Energy Lett* 5, 1371–1379.
- Hewlett, R.M., and McLachlan, M.A. (2016). Surface structure modification of ZnO and the

- impact on electronic properties. *Adv. Mater.* **28**, 3893–3921.
- Hou, J., Inganäs, O., Friend, R.H., and Gao, F. (2018). Organic solar cells based on non-fullerene acceptors. *Nat. Mater.* **17**, 119.
- Hu, H., Ghasemi, M., Peng, Z., Zhang, J., Rech, J.J., You, W., Yan, H., and Ade, H. (2020). The role of demixing and crystallization kinetics on the stability of non-fullerene organic solar cells. *Adv. Mater.* **32**, 2005348.
- Jørgensen, M., Norrman, K., Gevorgyan, S.A., Tromholt, T., Andreasen, B., and Krebs, F.C. (2012). Stability of polymer solar cells. *Adv. Mater.* **24**, 580–612.
- Labanti, C., Sung, M.J., Luke, J., Kwon, S., Kumar, R., Hong, J., Kim, J., Bakulin, A.A., Kwon, S.-K., Kim, Y.-H., and Kim, J.-S. (2021). Selenium-substituted non-fullerene acceptors: a route to superior operational stability for organic bulk heterojunction solar cells. *ACS Nano* **15**, 7700–7712.
- Li, N., Perea, J.D., Kassar, T., Richter, M., Heumueller, T., Matt, G.J., Hou, Y., Güldal, N.S., Chen, H., Chen, S., et al. (2017). Abnormal strong burn-in degradation of highly efficient polymer solar cells caused by spinodal donor-acceptor demixing. *Nat. Commun.* **8**, 14541.
- Lin, Y., Wang, J., Zhang, Z.-G., Bai, H., Li, Y., Zhu, D., and Zhan, X. (2015). An electron acceptor challenging fullerenes for efficient polymer solar cells. *Adv. Mater.* **27**, 1170–1174.
- Lin, Y., Firdaus, Y., Isikgor, F.H., Nugraha, M.I., Yengel, E., Harrison, G.T., Hallani, R., El-Labban, A., Faber, H., Ma, C., et al. (2020). Self-assembled monolayer enables hole transport layer-free organic solar cells with 18% efficiency and improved operational stability. *ACS Energy Lett* **5**, 2935–2944.
- Linglong Ye, Y.C., Li, Chao, Wang, Zhaohui, Zhan, Xiaowei, and Sun, Yanming (2020). Ferrocene as a highly volatile solid additive in non-fullerene organic solar cells with enhanced photovoltaic performance. *Energ. Environ. Sci.* **13**, 5117–5125.
- Liu, X., Li, X., Li, Y., Song, C., Zhu, L., Zhang, W., Wang, H.-Q., and Fang, J. (2016). High-performance polymer solar cells with PCE of 10.42% via Al-doped ZnO cathode interlayer. *Adv. Mater.* **28**, 7405–7412.
- Liu, X., Wang, H.-Q., Li, Y., Gui, Z., Ming, S., Usman, K., Zhang, W., and Fang, J. (2017). Regular organic solar cells with efficiency over 10% and promoted stability by ligand- and thermal annealing-free Al-doped ZnO cathode interlayer. *Adv. Sci.* **4**, 1700053.
- Liu, P., Wang, Y., Hao, H., Basu, S., Feng, X., Xu, Y., Boscoboinik, J.A., Nanda, J., Watt, J., and Mitlin, D. (2020a). Stable potassium metal anodes with an all-aluminum current collector through improved electrolyte wetting. *Adv. Mater.* **32**, 2002908.
- Liu, Q.S., Jiang, Y.F., Jin, K., Qin, J.Q., Xu, J.G., Li, W.T., Xiong, J., Liu, J.F., Xiao, Z., Sun, K., et al. (2020b). 18% Efficiency organic solar cells. *Sci. Bull.* **65**, 272–275.
- Mateker, W.R., and McGehee, M.D. (2017). Progress in understanding degradation mechanisms and improving stability in organic photovoltaics. *Adv. Mater.* **29**, 1603940.
- Mihailetchi, V.D., Blom, P.W.M., Hummelen, J.C., and Rispen, M.T. (2003). Cathode dependence of the open-circuit voltage of polymer:fullerene bulk heterojunction solar cells. *J. Appl. Phys.* **94**, 6849–6854.
- Park, S., Ahn, H., Kim, J.-Y., Park, J.B., Kim, J., Im, S.H., and Son, H.J. (2020). High-performance and stable nonfullerene acceptor-based organic solar cells for indoor to outdoor light. *ACS Energy Lett* **5**, 170–179.
- Rafique, S., Abdullah, S.M., Sulaiman, K., and Iwamoto, M. (2018). Fundamentals of bulk heterojunction organic solar cells: an overview of stability/degradation issues and strategies for improvement. *Renew. Sust. Energ. Rev.* **84**, 43–53.
- Speller, E.M., Clarke, A.J., Luke, J., Lee, H.K.H., Durrant, J.R., Li, N., Wang, T., Wong, H.C., Kim, J.-S., Tsoi, W.C., and Li, Z. (2019). From fullerene acceptors to non-fullerene acceptors: prospects and challenges in the stability of organic solar cells. *J. Mater. Chem. A* **7**, 23361–23377.
- Sun, R., Wu, Y., Guo, J., Wang, Y., Qin, F., Shen, B., Li, D., Wang, T., Li, Y., Zhou, Y., et al. (2021). High-performance all-small-molecule organic solar cells without interlayers. *Energ. Environ. Sci.* **14**, 3174–3183.
- Wang, H.-Q., Wang, S., Chen, L., Yin, Z., Mei, S., Zhong, Y., Yao, Y., Li, N., Wang, J., and Song, W. (2021). Understanding degradation mechanisms of perovskite solar cells due to electrochemical metallization effect. *Sol. Energ. Mat. Sol. C* **230**, 111278.
- Yang, W.Y., Luo, Z.H., Sun, R., Guo, J., Wang, T., Wu, Y., Wang, W., Guo, J., Wu, Q., Shi, M.M., et al. (2020). Simultaneous enhanced efficiency and thermal stability in organic solar cells from a polymer acceptor additive. *Nat. Commun.* **11**, 1218.
- Yao, J., Qiu, B.B., Zhang, Z.G., Xue, L.W., Wang, R., Zhang, C.F., Chen, S.S., Zhou, Q.J., Sun, C.K., Yang, C., et al. (2020). Cathode engineering with perylene-diimide interlayer enabling over 17% efficiency single-junction organic solar cells. *Nat. Commun.* **11**, 2726.
- Yin, Z.G., Wei, J.J., and Zheng, Q.D. (2016). Interfacial materials for organic solar cells: recent advances and perspectives. *Adv. Sci.* **3**, 1500362.
- Yu, Z.-P., Liu, Z.-X., Chen, F.-X., Qin, R., Lau, T.-K., Yin, J.-L., Kong, X., Lu, X., Shi, M., Li, C.-Z., and Chen, H. (2019). Simple non-fused electron acceptors for efficient and stable organic solar cells. *Nat. Commun.* **10**, 2152.
- Yuan, J., Zhang, Y., Zhou, L., Zhang, G., Yip, H.-L., Lau, T.-k., Lu, X., Zhu, C., Peng, H., Johnson, P.A., et al. (2019). Single-Junction organic solar cell with over 15% efficiency using fused-ring acceptor with electron-deficient core. *Joule* **3**, 1140–1151.
- Zhan, L., Li, S., Xia, X., Li, Y., Lu, X., Zuo, L., Shi, M., and Chen, H. (2021). Layer-by-Layer processed ternary organic photovoltaics with efficiency over 18%. *Adv. Mater.* **33**, 2007231.
- Zhang, M., Guo, X., Ma, W., Ade, H., and Hou, J. (2015). A large-bandgap conjugated polymer for versatile photovoltaic applications with high performance. *Adv. Mater.* **27**, 4655–4660.
- Zhang, C., Mumyatov, A., Langner, S., Perea, J.D., Kassar, T., Min, J., Ke, L., Chen, H., Gerasimov, K.L., Anokhin, D.V., et al. (2017). Overcoming the thermal instability of efficient polymer solar cells by employing novel fullerene-based acceptors. *Adv. Energy Mater.* **7**, 1601204.
- Zhang, C., Heumueller, T., Leon, S., Gruber, W., Burlafinger, K., Tang, X., Perea, J., Wabra, I., Hirsch, A., Unruh, T., et al. (2019). A top-down strategy identifying molecular phase stabilizers to overcome microstructure instabilities in organic solar cells. *Energ. Environ. Sci.* **12**, 1078–1087.
- Zhang, L., Huang, X., Duan, C., Peng, Z., Ye, L., Kirby, N., Huang, F., and Cao, Y. (2021). Morphology evolution with polymer chain propagation and its impacts on device performance and stability of non-fullerene solar cells. *J. Mater. Chem. A* **9**, 556–565.
- Zhao, L., Kerner, R.A., Xiao, Z., Lin, Y.L., Lee, K.M., Schwartz, J., and Rand, B.P. (2016). Redox chemistry dominates the degradation and decomposition of metal halide perovskite optoelectronic devices. *ACS Energy Lett* **1**, 595–602.
- Zheng, Z., Yao, H., Ye, L., Xu, Y., Zhang, S., and Hou, J. (2019). PBDB-T and its derivatives: a family of polymer donors enables over 17% efficiency in organic photovoltaics. *Mater. Today* **35**, 115–130.

STAR★METHODS

KEY RESOURCE TABLE

REAGENT or RESOURCE	SOURCE	IDENTIFIER
Chemicals and reagents		
PM6	Solarmer Materials Inc.	CAS#1802013-84-8
BTP-eC9	Solarmer Materials Inc.	CAS#NA
PEDOT:PSS	J&K Scientific	CAS#155090-83-8
PFN-Br	Solarmer Materials Inc.	CAS#889672-99-5
Aluminum nitrate monohydrate	Sinopharm Chemical Reagent Co.	CAS#7784-27-2
zinc acetate dihydrate		CAS#557-34-6
potassium hydroxide		CAS#1310-58-3
Chloroform	Sigma-Aldrich	CAS#865-49-6
1-chloronaphthalene	Sigma-Aldrich	CAS#90-13-1
Trifluoroethanol	Sigma-Aldrich	CAS#75-89-8
Silver/Aluminium	Zhongnuo New Material Technology Co.	CAS#Ag13402 CAS#Al13501
ITO substrate	Shenzhen huayulianhe Technology Co.	CAS#NA

RESOURCE AVAILABILITY

Lead contact

Further information and requests for resources and reagents should be directed to and will be fulfilled by the lead contact, Hai-Qiao Wang (hqwang@nimte.ac.cn)

Materials availability

This study did not generate new, unique reagents. Any additional information about the device fabrication, tests and conditions reported in this paper is available from the lead contact upon request.

Data and code availability

All data have been provided in the paper or Supplemental Information.

This study did not generate any other specific data.

Any additional information required to reanalyze the data reported in this paper is available from the lead contact upon request.

METHOD DETAILS

Materials and reagents

Patterned ITO glass substrates ($R_s \leq 10 \Omega/\square$, $T\% \geq 83\%$) were provided by Shenzhen huayulianhe Technology Co. Organic active materials PM6 and BTP-eC9 were obtained from Solarmer Materials Inc. Aluminum nitrate monohydrate ($\text{Al}(\text{NO}_3)_3 \cdot 9\text{H}_2\text{O}$), zinc acetate dihydrate ($\text{Zn}(\text{Ac})_2 \cdot 2\text{H}_2\text{O}$), and potassium hydroxide (KOH) were purchased from Sinopharm Chemical Reagent Co. Chloroform (CF), 1-chloronaphthalene (CN) and TFE were bought from Sigma-Aldrich. All the available chemical reagents were used as received without any further purification. The AZO nanoparticles were synthesized with a modified method according to published literature (Liu et al., 2017).

Device fabrication

The ITO-coated glass substrates were cleaned by sequential sonication in detergent, deionized water, acetone, and isopropanol for 15 min at each step. Then the pre-cleaned ITO substrates were treated with oxygen plasma for 10 min. A PEDOT:PSS (Baytron, Clevious 4083) aqueous solution was spin-coated

onto the ITO substrates and then annealed in air at 140 °C for 20 min. Next, the active layer was deposited by spin coating from a PM6:BTP-eC9 (1:1.2 wt%, 16 mg/mL) solution in the mixed solvent of CF:CN (99.5:0.5 vol%) under 3500 rpm for 40 s. Then the AZO solution (in TFE) was spin-coated onto the active layer at 5000 rpm for 60 s. The PFN-Br solution (0.5 mg/ml in methanol) was spin-coated onto the active layer at 4000 rpm for 30 s and the PDINN solution (1 mg/ml in methanol) was spin-coated onto the active layer at 4000 rpm for 30 s. Then the devices were immediately put into the chamber for electrode deposition. Finally, the device fabrication was completed by thermal evaporation of 100 nm Al or Ag as the electrode under a pressure less than 4×10^{-4} Pa. The effective device area was defined to be 0.06 cm² controlled with a shadow mask.

Characterizations

The current density-voltage characteristics were measured inside an N₂-filled glove box, using a Keithley 2400 source meter under the illumination of AM 1.5G (100 mW cm⁻²), with a Sol3A class AAA solar simulator (Newport, model 94023A, 2×2 in.). The lamp was calibrated by a 2×2 cm² mono-crystalline silicon reference cell (KG5 filter) provided by Newport Corporation. XPS measurements were carried out using a Kratos AXIS ULTRA DALD XPS system. For XPS, survey scans were recorded using a monochromatic Al K α X-ray source (1486.6 eV) to determine surface metal valence changes. For operational stability test, white LED (spectra region: 430-800 nm, Suzhou D&R instruments Co., Ltd. PVL-6001M-16A) was continuously applied to the device for illumination. Its intensity was adjusted in a way that the generated photocurrent matched the one under a solar simulator. A semiconductor refrigeration technique was applied to control the device temperature below 30 °C in the aging process to avoid heat influence. The moisture and O₂ concentrations were kept below 0.1 p.p.m foraging in the N₂ glove box. J-V scan was conducted *in situ* (without moving the devices) every 30 minutes to trace the performance and MPP point. A variable resistor as the load was introduced to connect with the device immediately after each J-V scan, to make the device always work at MPP. It should be noted that the decay curve starts to record once the device is subjected to aging. It means all decay processes are contained in the decay curve, including burn-in loss.

QUANTIFICATION AND STATISTICAL ANALYSIS

The data in this manuscript are shown as the means \pm SD.